Nadimi, S. & Fonseca, J. *Géotechnique* [http://dx.doi.org/10.1680/jgeot.16.P.163]

TECHNICAL NOTE

A micro finite-element model for soil behaviour: numerical validation

S. NADIMI* and J. FONSECA†

A micro finite-element (μFE) model capable of handling arbitrary shapes and deformable grains has been developed by the authors. The basis of this μFE model is to use a virtualised soil fabric obtained from micro computed tomography (μCT) of real sand to simulate grain-to-grain interaction in a framework of combined discrete–finite-element method. By incorporating grain deformation into the model, the contact response emerges from the interaction of contacting bodies and each irregular contact area will produce a unique response. A detailed numerical description of grain morphology and contact topology of a natural sand and the subsequent simulation are presented in the original paper. The present study focuses on the numerical validation of the constitutive contact behaviour against existent theories, for a single sphere and an assembly of spheres. The ability of the model to simulate elastic–plastic behaviour making use of the deformability of the grains is demonstrated. The unloading–reloading behaviour associated with the geometrical arrangement of the grains for a granular assembly under triaxial compression is examined in terms of energy dissipation quantities.

KEYWORDS: fabric/structure of soils; particle-scale behaviour; numerical modelling; sands

INTRODUCTION

The irregular shape of sand particles originates complex contact topologies (e.g. Fonseca *et al.*, 2013), which differ significantly from the point contact condition assumed for deriving theoretical contact laws (Thornton, 2015). This implies that the ideal shapes and conventional contact laws used for the most part in discrete-element method (DEM) studies may be of limited application to model real sand. According to previous experimental studies (e.g. Cavarretta, 2009; Cavarretta *et al.*, 2010; Cole *et al.*, 2010; Senetakis *et al.*, 2013), contact response depends not only on contact topology, but also on previous loading history and deformation mechanisms that the grain undergoes during rearrangement under loading. In addition, particle rearrangements computed based on inter-particle penetration in DEM may lead to the misrepresentation of the kinematics in granular media.

The micro finite-element (μFE) model (Nadimi & Fonseca, 2017) was developed with the aim of providing a more realistic representation of the physics of granular behaviour by incorporating the actual particle morphology and contact topology of real soil into deformable numerical grains. One advantage of representing grains as deformable bodies is the possibility of introducing plasticity at the grain-scale. Continuum deformable representation of ideal shapes using finite elements has been considered previously, particularly in powder technology (e.g. Harthong *et al.*, 2009; Nezamabadi *et al.*, 2015; Rathbone *et al.*, 2015). The use of combined finite–discrete approaches to model systems of spheres is, however, not well established. This paper fills this gap by providing the numerical validation of the μFE model for an assembly of spheres. Moreover, the finite-element (FE) discretisation is assessed for a single sphere and the elastic–plastic behaviour of a granular system is simulated under triaxial compression.

Manuscript received 27 June 2016; revised manuscript accepted 22 June 2017.
Discussion on this paper is welcomed by the editor.
* Department of Civil Engineering, City, University of London, London, UK (Orcid:0000-0002-0971-7089).
† Department of Civil Engineering, City, University of London, London, UK (Orcid:0000-0002-7654-6005).

BEHAVIOUR OF A SINGLE SPHERE

The problem here consists of modelling the contact between two identical spheres under loading (Fig. 1). The material parameters used in the simulation are listed in Table 1. An explicit integration scheme was employed so that the same procedure can be used to simulate an assembly of grains (Nadimi & Fonseca, 2017). The properties of hard contact behaviour – that is, all the force is transmitted through the contact – were defined between the two contacting bodies.

Mesh size effect

The simulation results are mesh size dependent. Although using a very fine mesh will yield more accurate results, the computational cost involved to simulate a large assembly of grains would require optimising the mesh size value. In order to investigate the effect of mesh size and find the optimal value, a range of mesh sizes were examined. The size of the mesh is quantified using the meshing ratio (MR) parameter, defined as follows

$$\mathrm{MR} = s/2R \tag{1}$$

where s is the seeding distance and R is the sphere's radius.

An example of a seeding distance of 0·1 on a sphere with a radius of 1·1 mm, which leads to 70 seeds along one perimeter, is presented in Fig. 2(a). Figs 2(b), 2(c) and 2(d) show examples of three spheres with different meshing ratio used in this study.

Normal loading

Hertz theory provides a relationship between normal force (F_N) and displacement for two elastic spheres in contact

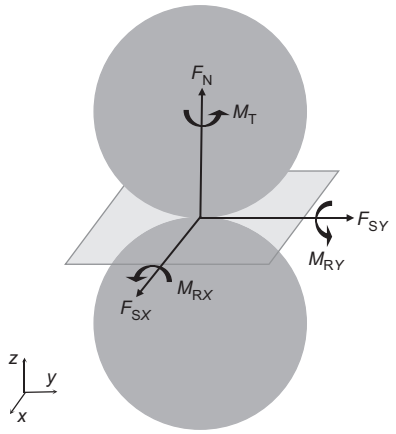

Fig. 1. Transmitting forces and moments between two spheres in contact: normal force (F_N), two tangential forces (F_{SX} and F_{SY}), twisting (M_T) and rolling moments (M_{RY} and M_{RX})

Table 1. Material parameters used in the simulations

Parameter	Symbol	Value	Units
Young's modulus	E	63	GPa
Poisson's ratio	ν	0·22	—
Density	ρ	2·5	t/m^3
Coefficient of friction	μ	0·22	—

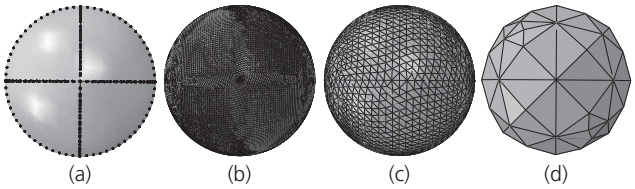

Fig. 2. (a) Seeding along three perimetrical edges of a sphere and three examples of different meshing ratios: (b) MR = 0·014; (c) MR = 0·045; (d) MR = 0·364

(Hertz, 1882). In this case, F_N can be determined from the following equation

$$F_N = \int\int_S \sigma_{zz} \mathrm{d}s = F_{\mathrm{Hertz}} = \frac{4}{3} E^* \sqrt{R} \delta_n^{3/2} \tag{2}$$

where E^* is the effective contact stiffness given by $E^* = E/(1-\nu^2)$, R is the sphere's radius, δ_n is the normal displacement, S denotes the contact area, E is the elastic modulus and ν is the Poisson's ratio.

The simulation of an elastic sphere under normal loading was conducted using different meshing ratios, as shown in Fig. 3. As the mesh becomes more refined for MR increasing values of 0·090, 0·045 and 0·014, no significant difference can be observed in comparison with the reference results. Only for very coarse meshing, that is, MR = 0·364, is a very dissimilar response observed.

Tangential loading

Mindlin (1949) and Mindlin & Deresiewicz (1953) investigated the elastic deformation of two contacting spheres under tangential loading. Based on their results, the tangential force–displacement can be described as follows

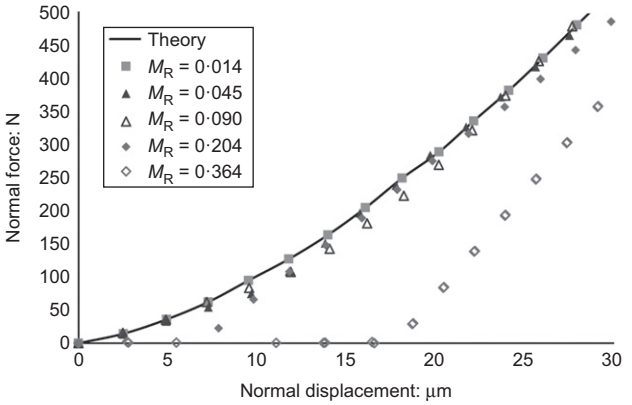

Fig. 3. Effect of the meshing ratio on normal loading of an elastic sphere

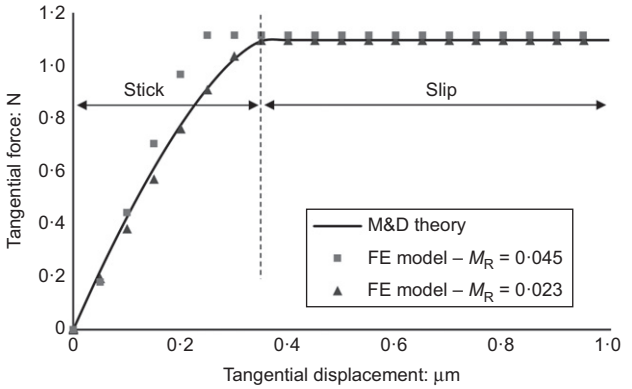

Fig. 4. The effect of meshing ratio on the tangential response of a sphere, $F_N = 5$ N

$$F_{\mathrm{M\&D}} = \int\int_s \sigma_{xy} \mathrm{d}s = \mu F_N \left\{ 1 - \left[1 - \frac{\min(|\delta_t|,\ \delta_{t\,\max})}{\delta_{t\,\max}} \right]^{3/2} \right\} \tag{3}$$

where μ is the friction coefficient, $\delta_{t\,\max}$ is the maximum tangential deflection before sliding, $\delta_{t\,\max} = 0{\cdot}5\mu\delta_n(2-\nu)/(1-\nu)$, and when $|\delta_t| \geq \delta_{t\,\max}$ sliding occurs.

Tangential loading was applied to the sphere, under a constant normal load $F_N = 5$ N, for MR = 0·045 and MR = 0·023. Fig. 4 shows the tangential force–displacement obtained using the results from the μFE against the Mindlin and Deresiewicz (M&D) theory; in this plot two distinct regions can be identified: the 'stick' region and the 'slip' region. A perfect agreement can be observed for a MR = 0·023. The very small discrepancy in the sticking region, in this case of MR = 0·045 for a tangential displacement between 0·2 μm and 0·4 μm, is related to mesh size only.

Torsional loading

Torsional loading is defined as the twisting moment (M_T) around the axis of the contact normal. When M_T is applied in combination with normal loading to an elastic sphere, the contact area will undergo rotation (given by the angle β). The frictional forces at the contact will provide some resistance to sliding. The region that meets the Coulomb's friction condition will experience sliding and the rest of the contact area will undergo sticking according to the normal forces distribution (Dintwa *et al.*, 2005). Lubkin (1951) provides the

solution to this problem by proposing an equation to determine the shear stress at the contact surface within the stick region, using elliptical integrals. The complexity of Lubkin's solution was simplified by Deresiewicz (1954) by proposing an explicit approximation between a, M_T and β for simple implementation, defined as follows

$$\frac{Ga^2\beta}{\mu F_N} = \frac{1}{8}\left[1 - \sqrt{1 - \frac{3}{2}\frac{M_T}{\mu F_N a}}\right] \times \left[3 - \sqrt{1 - \frac{3}{2}\frac{M_T}{\mu F_N a}}\right] \quad (4)$$

where G is the shear modulus.

The comparison of the μFE results for different meshing ratio values against Deresiewicz theory is presented in Fig. 5. It can be observed that, although for a mesh ratio of 0·045 there is a large discrepancy between the theoretical and the FE model curves, for finer mesh ratios, of 0·014 and 0·023, a good agreement is shown.

Rotational loading

Rolling resistance or friction is related to energy dissipation due to an asymmetric stress distribution at the contact area. When the stress distribution at the front of the contact region is higher than at the back, this originates a resistance moment, termed rolling resistance. Similarly to the case for M_T, the coexistence of slip and stick zones makes the calculation of the rolling moment less trivial. Considering a very small angle of rotation, Johnson (1985) proposed a creep model to calculate the difference between the tangential strains in both the stick and slip areas. For a circular contact area and under a transmitting traction Q_x, creep is given by

$$\varepsilon_x = -\frac{3\mu F_N(4-3\nu)}{16Ga^2}\left[1 - \left(1 - \frac{Q_x}{\mu F_N}\right)^{1/3}\right] \quad (5)$$

and when under transmitting traction Q_y, creep is obtained as follows

$$\varepsilon_y = -\frac{3\mu F_N(4-\nu)}{16Ga^2}\left[1 - \left(1 - \frac{Q_y}{\mu F_N}\right)^{1/3}\right] \quad (6)$$

The problem of purely rolling for two spheres in contact was simulated in the μFE model under constant normal loading of 70 N. The results of this simulation were compared with Johnson's theory and depicted in Fig. 6. Similarly to the observations for the torsional loading, although some discrepancy can be observed for an MR of 0·045, for MR values of 0·014 and 0·023 a good agreement between the curves is shown. Here, the rolling resistance is

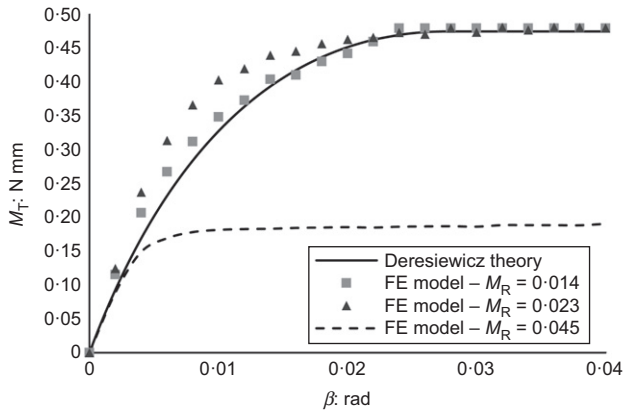

Fig. 5. The effect of meshing ratio on the relationship torque plotted against twisting angle, for an elastic sphere under $F_N = 40$ N

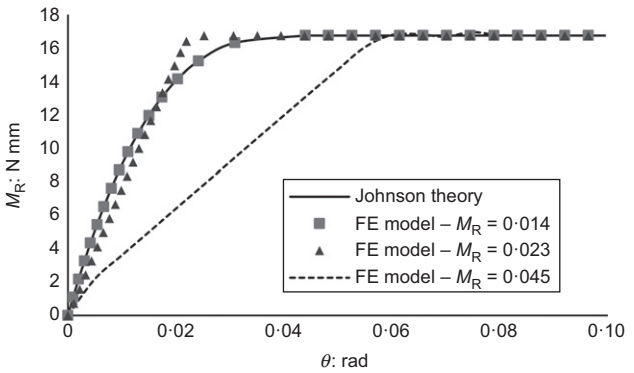

Fig. 6. Rolling moment plotted against rotational angle under constant normal force $F_N = 70$ N

derived from the actual rotational moment between two contacting bodies, which differs from the artificial rolling resistance used in previous studies to account for the effect of grain shape (Iwashita & Oda, 1998; Jiang *et al*., 2005).

BEHAVIOUR OF AN ASSEMBLY OF SPHERES

This section investigates the ability of the model to simulate the response of an assembly of spheres subjected to triaxial compression. First, pure elastic behaviour is assigned to the model, which allows comparison with the theoretical response. The response of the assembly is subsequently investigated using an elastic–plastic model.

Model description

A specimen of 2000 uniform spheres with radius of 1·1 mm and prepared with a face-centred cubic (FCC) packing, was generated within the μFE framework. This FCC packing was chosen so that the analytical failure method proposed by Thornton (1979) for an FCC array of uniform rigid spheres under triaxial compression can be used (e.g. O'Sullivan *et al*., 2004; Barreto, 2010; Huang, 2014). Frictionless rigid boundaries were applied to the triaxial sample. A hybrid mesh of fine elements at the surface (MR = 0·045) and coarser elements inside the sphere was adopted to reduce the computational cost of the simulation without compromising the accuracy of the results. In total, the model contains 16 197 200 elements and 4 099 372 nodes. The loading process comprises isotropic compression at 50 kPa followed by shearing under controlled strain. The full simulation took approximately 24 h running on a Dell Precision T7610.

Elastic behaviour

The material parameters used in this simulation are indicated in Table 1. Under elastic conditions the failure of the system is believed to occur as a result of the formation of a gap between the initially contiguous spheres. According to Thornton's solution this so-called 'failure' is expected to occur at $\sigma_1 = 156{\cdot}4$ kPa. In the μFE it was seen to occur at $\sigma_1 = 162{\cdot}5$ kPa (Fig. 7(a)). The small difference between these σ_1 values can be attributed to the effect of the rigid boundaries used in the μFE simulation when compared with the infinite boundaries considered in the theoretical formulation. The simulation was run for four additional coefficient of friction values (0·3, 0·4, 0·5 and 0·6) and the measured stress ratio σ_1/σ_3 was compared with the theoretical results. A very good agreement can be observed between the

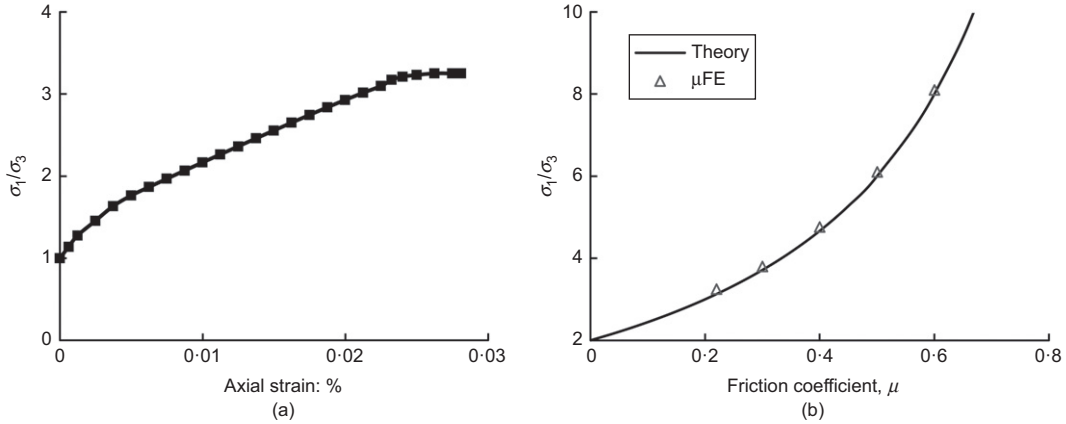

Fig. 7. μFE results for a triaxial test on FCC packed elastic spheres: (a) stress ratio plotted against axial strain response; (b) comparison with Thornton's theory in terms of stress ratio plotted against friction coefficient

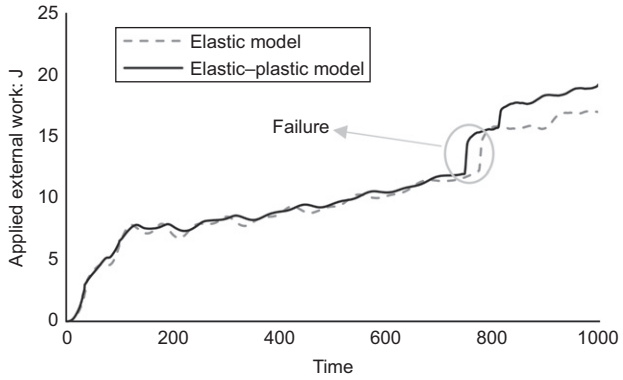

Fig. 8. Applied external work plotted against time for elastic and elastic–plastic models ($\mu = 0{\cdot}22$)

response from the μFE model and Thornton's theory as shown in Fig. 7(b).

Elastic–plastic behaviour

Energy may be dissipated by plastic deformation of the contacting bodies which leads to residual deformation and significantly affects reloading of that particular contact area. Plastic behaviour is introduced for the assembly using an isotropic hardening model with 100 MPa yield stress applied to all particles, similarly to what has been described previously. Failure was observed to occur at $\sigma_1 = 158$ kPa – that is, a slightly lower value when compared with the pure elastic case. The response of the elastic and the elastic–plastic models was compared in terms of energy quantities. The energy balance for the model can be obtained according to the first law of thermodynamics. Fig. 8 shows the evolution of the applied external work with time for both elastic and elastic–plastic models. It can be seen that failure occurs earlier in the elastic–plastic simulation and after failure the external work is also greater for the elastic–plastic case. In order to further investigate the contribution of plasticity, the authors compared recoverable and internal energy and also plastic dissipation and frictional dissipation for both the elastic and the elastic–plastic models. Fig. 9(a) shows that all the internal strain energy is recoverable for the elastic simulation (as shown by the overlapping of the two curves), whereas only approximately one-third of the energy is recoverable in the plastic simulation. This is an indicator of the significant contribution of plasticity on unloading of the grains under shearing. In the elastic–plastic model presented,

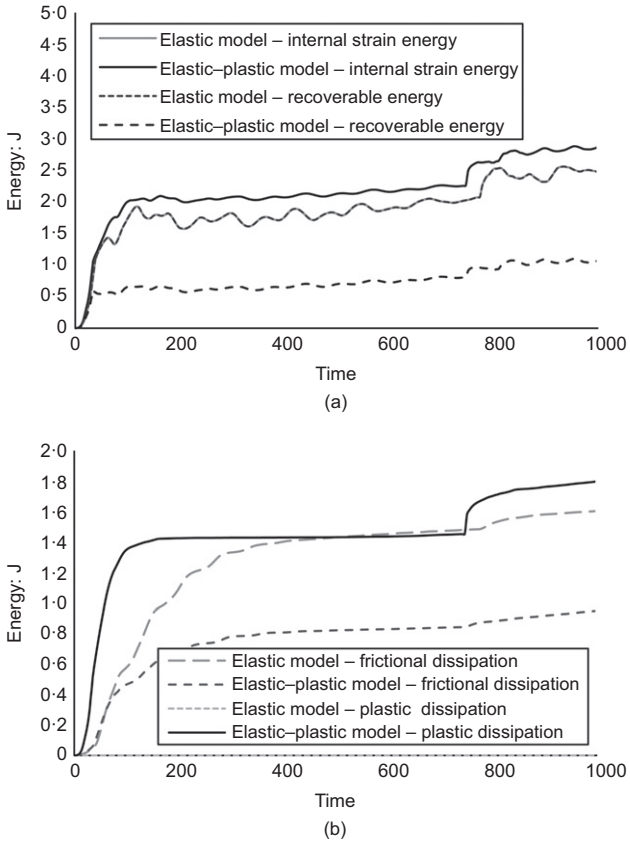

Fig. 9. (a) Comparison of the internal strain energy with recoverable strain energy for both elastic and elastic–plastic models; (b) comparison of frictional and plastic energy dissipation ($\mu = 0{\cdot}22$)

the contribution of plastic dissipation is twice the frictional dissipation as depicted in Fig. 9(b). The plastic dissipation curve in Fig. 9(b) also suggests the creation of a new plastic contact surface between the grains that became detached at failure. These observations emphasise the need to include plasticity for discrete simulation of granular media.

Figure 10 shows the distribution of elastic and plastic energy dissipation for the case of a single grain in Hertzian contact. Based on this, Amini *et al*. (2015) recently proposed a plastic dissipated energy index for a single elastic–plastic particle given by the ratio between plastic and total contact energy (i.e. the sum of elastic and plastic energies). Using the same concept, a friction dissipated energy index is introduced

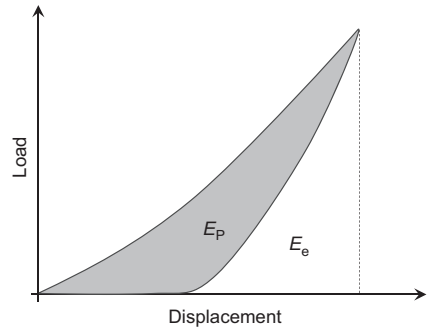

Fig. 10. Energy dissipation by plastic yielding during a Hertzian contact cycle, E_e is the elastic energy and E_P is the plastic energy (after Amini *et al.*, 2015)

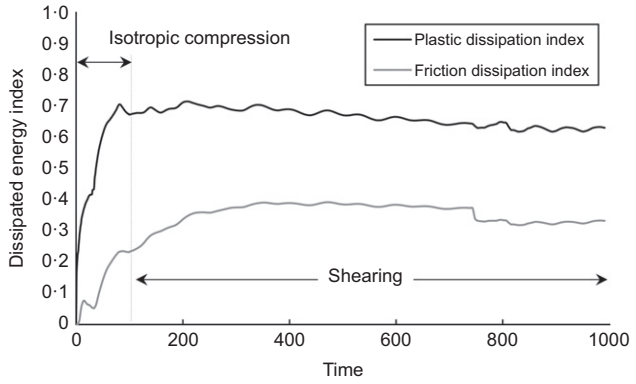

Fig. 11. Dissipated energy index for an elastic–plastic assembly of spheres

here, defined as the ratio between friction energy and total energy. The evolution of those two indices is presented in Fig. 11. It can be seen that the plastic index shows a high increase during isotropic compression and exhibits only small fluctuation in the shearing stage. The friction index continues to increase at the beginning of shearing and shows a little drop at failure. Overall, the plastic energy contribution is higher than the frictional energy dissipation, for this loading scenario.

CONCLUSIONS

The ability of the μFE model to simulate contact behaviour for a system of spheres was demonstrated here by comparison with theoretical formulations. Mesh size dependency was investigated and a hybrid mesh was proposed to improve the computation cost of the simulation. Since contact interaction is modelled based on the deformation of the contacting area and an assigned friction coefficient, this avoids the use of complex contact laws and presents a clear improvement for modelling irregular-shaped particles with complex contact topology found in real sand. Dissipated energy indices for friction and plastic behaviour are introduced to quantify energy dissipation due to unloading–reloading of contacts during grain rearrangement. For the case of an assembly of regularly packed spheres under triaxial compression, the greater contribution of plasticity when compared to friction was shown. The results from the simulations presented here illustrate the potential of the μFE approach to simulate more realistic contact interaction of granular media, including soil.

ACKNOWLEDGEMENTS

The authors would like to thank City University of London for the doctoral scholarship of the first author and express gratitude to Dr Tom Shire from Imperial College London, for his suggestions on the last section of the paper.

NOTATION

a	radius of contact area
E	elastic modulus
E^*	effective contact stiffness
E_e	elastic energy
E_P	plastic energy
E_t	hardening modulus
$F_{M\&D}$	tangential contact force
F_N	normal contact force
G	shear modulus
M_R	rolling moment
M_T	twisting moment
Q_x	traction force in x-direction
Q_y	traction force in y-direction
R	radius of sphere
S	contact interface/area
s	seeding distance
U	internal energy per unit mass
β	twisting angle
δ_n	normal displacement
δ_t	tangential deflection
$\delta_{t\,max}$	maximum tangential deflection
ν	Poisson's ratio
μ	friction coefficient
ρ	density
σ_{xy}	shear stress in xy plane along the y-axis
σ_{zz}	normal stress along the z-axis

REFERENCES

Amini, S., Tadayon, M., Idapalapati, S. & Miserez, A. (2015). The role of quasi-plasticity in the extreme contact damage tolerance of the stomatopod dactyl club. *Nature Mater.* **14**, No. 9, 943–950.

Barreto, D. (2010). *Numerical and experimental investigation into the behaviour of granular materials under generalised stress states.* PhD thesis, Imperial College London, London, UK

Cavarretta, I. (2009). *The influence of particle characteristics on the engineering behaviour of granular materials.* PhD thesis, Imperial College London, London, UK.

Cavarretta, I., Coop, M. & O'Sullivan, C. (2010). The influence of particle characteristics on the behaviour of coarse grained soils. *Géotechnique* **60**, No. 6, 413–423, http://dx.doi.org/10.1680/geot.2010.60.6.413.

Cole, D. M., Mathisen, L. U., Hopkinks, M. A. & Knapp, B. R. (2010). Normal and sliding contact experiments on gneiss. *Granular Matter* **12**, No. 1, 69–86.

Deresiewicz, H. (1954). Contact of elastic spheres under an oscillating torsional couple. *ASME J. Appl. Mech.* **21**, No. 1, 52–56.

Dintwa, E., Zeebroeck, M. V., Tijskens, E. & Ramon, H. (2005). Torsion of viscoelastic spheres in contact. *Granular Matter* **7**, No. 2–3, 169–179.

Fonseca, J., O'Sullivan, C., Coop, M. R. & Lee, P. D. (2013). Quantifying the evolution of soil fabric during shearing using scalar parameters. *Géotechnique* **63**, No. 10, 818–829, http://dx.doi.org/10.1680/geot.11.P.150.

Harthong, B., Jérier, J. F., Doremus, P., Imbault, D. & Donzé, F. V. (2009). Modelling of high-density compaction of granular materials by the discrete element method. *Int. J. Solids Structs* **46**, No. 18, 3357–3364.

Hertz, H. (1882). Über die Berührung fester elastischer Körper. *J. reine und angewandte Mathematik* **92**, 156–171 (in German).

Huang, X. (2014). *Exploring critical-state behaviour using DEM*. PhD thesis, University of Hong Kong and Imperial College London, London, UK.

Iwashita, K. & Oda, M. (1998). Rolling resistance contacts in simulation of shear band development by DEM. *J. Engng Mech.* **124**, No. 3, 285–292.

Jiang, M., Yu, H. S. & Harris, D. (2005). A novel discrete model for granular material incorporating rolling resistance. *Comput. Geotech.* **32**, No. 5, 340–357.

Johnson, K. L. (1985). *Contact mechanics*. Cambridge, UK: Cambridge University Press.

Lubkin, J. L. (1951). The torsion of elastic spheres in contact. *ASME J. Appl. Mech.* **18**, No. 2, 183–187.

Mindlin, R. D. (1949). Compliance of elastic bodies in contact. *ASME J. Appl. Mech.* **16**, 259–268.

Mindlin, R. D. & Deresiewicz, H. (1953). Elastic spheres in contact under varying oblique forces. *ASME J. Appl. Mech.* **20**, 327–344.

Nadimi, S. & Fonseca, J. (2017). A micro finite-element model for soil behaviour. *Géotechnique*, http://dx.doi.org/10.1680/jgeot.16.P.147

Nezamabadi, S., Radjai, F., Averseng, J. & Delenne, J. Y. (2015). Implicit frictional-contact model for soft particle systems. *J. Mech. Phys. Solids* **83**, 72–87.

O'Sullivan, C., Bray, J. D. & Riemer, M. (2004). Examination of the response of regularly packed specimens of spherical particles using physical tests and discrete element simulations. *J. Engng Mech. – ASCE* **130**, No. 10, 1140–1150.

Rathbone, D., Marigo, M., Dini, D. & van Wachem, B. (2015). An accurate force–displacement law for the modelling of elastic–plastic contacts in discrete element simulations. *Powder Technol.* **282**, 2–9.

Senetakis, K., Coop, M. & Todisco, C. (2013). The inter-particle coefficient of friction at the contacts of Leighton Buzzard sand quartz minerals. *Soils Found.* **53**, No. 5, 746–755.

Thornton, C. (1979). The conditions of failure of a face-centered cubic array of uniform rigid spheres. *Géotechnique* **29**, No. 4, 441–459, http://dx.doi.org/10.1680/geot.1979.29.4.441.

Thornton, C. (2015). *Granular dynamics, contact mechanics and particle system simulations*. Cham, Switzerland: Springer International.